Appendix 1

A1 EXPERIMENTAL DESIGN

A1.1 Constant Temperature vs. Dynamic Crystallization Experiments

The rationale for choosing to analyze controlled cooling instead of isothermal experimental charges to measure anorthite-melt divalent element partition coefficients has been discussed in chapter 2. The difference in crystal size produced by these two thermal regimes is illustrated by back-scattered electron (BSE) imaging in Figure A1.1, which shows that the short dimensions of anorthite laths grown under isothermal conditions rarely exceed 10 μm (a). As the 400 nA beam of the Caltech JEOL 733 electron microprobe had a diameter of ~12 μm, all reconnaissance trace element analyses of these small crystals included a glass component. Image (b) of the same composition shows crystals grown by dynamic crystallization, which are analyzed easily both by electron microprobe and ion probe.

Figure A1.1. Comparison of anorthite crystals grown under (a) isothermal conditions (run 2-2-8), and (b) a dynamic crystallization thermal regime (run 2b-2-2).

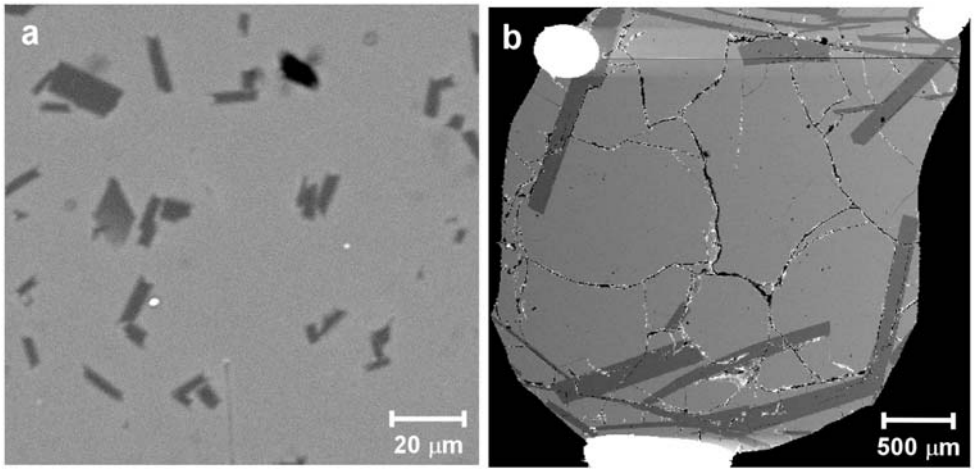

A graphical representation of the controlled cooling program discussed in Section 2.2.4, based on that of Simon et al. (1994), is shown below in Figure A1.2, with furnace temperature plotted as a function of time.

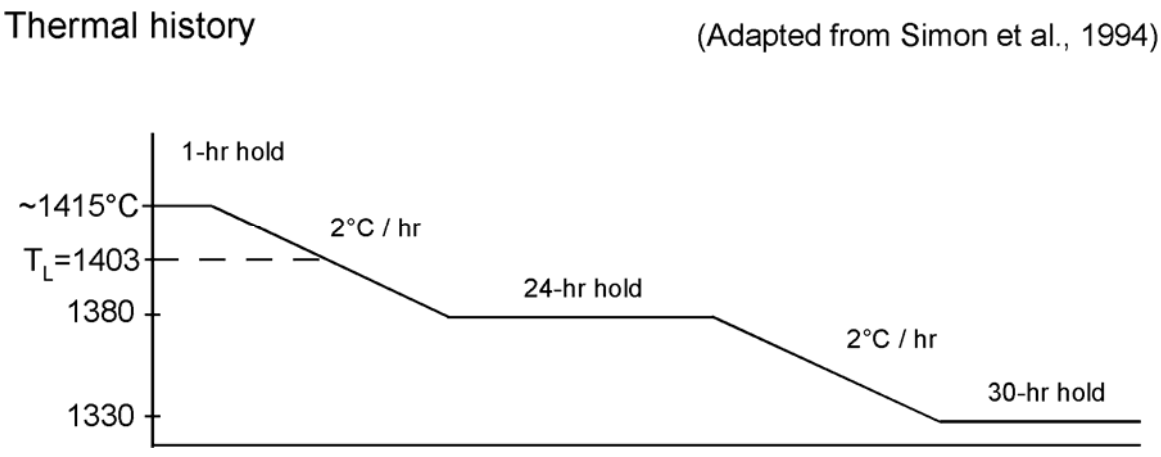

Figure A1.2. Controlled cooling path of dynamic crystallization experiments described in chapter 2.

A1.2 Comparison of Electron Probe and Ion Microprobe Analysis Data for CMAS2 Compositions

A1.2.1 CMAS2 Partitioning Data from Electron Microprobe Analysis of Crystal Centers

Several analytical methods, conditions, and starting material spike concentrations were considered when attempting to resolve the differences in barium, the most incompatible element of these studies, partitioning in the seven CMAS composition systems described in chapter 2. Anorthite crystal center points from compositions doped with 1500 ppm Ba were measured by electron microprobe analysis (EMP). Analytical

conditions were 25 nA and 15 keV, with 30 s on peak and 15 s background counting times and standards as listed in Section 2.2.4. Assuming that crystal centers represent anorthite that grew from the initial melt composition, partition coefficients were calculated using the compositions of fused glasses of the starting materials. While this may not be strictly true, it likely produces a better representation of partitioning near the anorthite liquidus than the apparent *D* value generated by crystal center/final melt data. The first column of Table A1.1 shows that the Ba partition coefficients calculated from these data have large uncertainties and are indistinguishable from one another.

The standard deviations given for the crystal center EMP D_{Ba} are essentially entirely due to the variability in the crystal EMP analyses. The higher Ba concentration, higher beam currents, and longer counting times for the rim EMP Ba data in Table A1.2.1 can explain the larger variability of the center EMP D_{Ba}. Nevertheless, the center EMP D_{Ba} values are systematically higher than the rim values for 6 of the 7 compositions. This is evidence for disequilibrium partitioning that reflects initial rapid crystal growth. The larger standard deviations for the center EMP Sr data are also explained by the differences in analytical conditions. Here, unlike Ba, there are no systematic differences between D_{Sr} values for the center and rim analyses of the different compositions, and the two data sets agree to within ± 15 %. With a partition coefficient near 1, Sr is very insensitive to disequilibrium effects associated with liquid boundary layers; however, if disequilibrium were due to a greater importance of surface, as opposed to bulk, partitioning at initially high growth rates, then Sr might have been as likely to show disequilibrium effects as any other element. Our next analytical approach involved

measuring trace element compositions of anorthite interiors from these same samples by ion microprobe.

Table A1.1. Comparison of three CMAS2 anorthite/melt molar partition coefficient data sets generated by electron microprobe and ion microprobe analysis of spots in the centers of crystals doped with 1500 ppm Ba and electron microprobe analysis of anorthite crystal edges from starting material doped with 3000 ppm Ba. Not analyzed = na.

	Ba			Sr			Be
Crystal Data Location	Center	Center	Rim	Center	Center	Rim	Center
Instrument	EMP	SIMS	EMP	EMP	SIMS	EMP	SIMS
Beam	25 nA	2 nA	400 nA	25 nA	2 nA	400 nA	2 nA
Doping concentration	1500 ppm	1500 ppm	3000 ppm	1000 ppm	1000 ppm	1000 ppm	500 ppm
2-1	0.23 (28)	0.20 (2)	0.18 (2)	0.78 (28)	1.01 (2)	0.90 (5)	0.27 (2)
2-2	0.21 (22)	0.20 (2)	0.15 (2)	0.77 (24)	1.03 (4)	0.92 (4)	0.22 (4)
2-3	0.18 (21)	0.20 (3)	0.16 (1)	0.90 (24)	1.14 (6)	0.97 (5)	0.21 (2)
2-4	0.33 (20)	0.16 (2)	0.18 (2)	0.98 (26)	1.13 (2)	1.06 (5)	0.153 (3)
2-5	0.27 (22)	0.23 (1)	0.18 (1)	1.29 (42)	1.34 (3)	1.16 (5)	0.138 (7)
2-6	0.26 (22)	0.19 (2)	0.18 (1)	1.49 (52)	1.37 (2)	1.29 (4)	0.13 (1)
2-7	0.13 (14)	na	0.21 (2)	1.43 (40)	na	1.45 (6)	na

A1.2.2 CMAS2 Partitioning Data from Ion Microprobe Analysis of Crystal Centers

Anorthite and coexisting glass from the seven compositions of the CMAS2 series were analyzed with the Lawrence Livermore National Laboratory (LLNL) Cameca ims-3f ion microprobe (SIMS). The primary beam had 12.5 kV, 2 nA primary beam, a 4500 V secondary accelerating voltage, and a 60 V offset to minimize molecular ion interferences. Ion count rates were normalized to ^{40}Ca and converted to concentration factors determined from several glass standards. A CMAS+Ti glass from run 224SAM21 containing 1.65 +/- 0.13 wt. % Ba as determined on the Caltech 733 JEOL electron microprobe was used as a Ba standard and TI-G quartz diorite glass with 2.4 ppm Be served as a Be standard.

The concentration of a trace element measured by SIMS may be calculated from the following equation:

$$C_i(\text{ppm}) = F\left(\frac{I_i}{I_{^{40}Ca}}\right)\left(\frac{CaO_i}{CaO_{std}}\right). \quad \text{(A1)}$$

F represents a calibration factor, I_i is the ion intensity of the trace element of interest (*i*) (counts/s), $I_{^{40}Ca}$ is the measured ion intensity for ^{40}Ca, CaO_i is the concentration of CaO in the sample material, and CaO_{std} is the CaO concentration in the standard for which the calibration factor was determined. The success of F accurately converting measured ion intensity of the trace element into concentration depends on how similar ^{40}Ca sputtering is to that of the trace element *i*.

The SIMS analyses generated more precise Ba and Sr data, but subsequent 400 nA analyses of points within and around several ion probe analysis pits, which were 30–50 μm in diameter, indicated nontrivial heterogeneity in the anorthite crystals that would not be spatially well resolved by ion probe. Since the electron microprobe has a more focused beam than the ion probe even at 400 nA, the trace element partitioning study of chapter 2 was conducted using starting materials doped with 3000 ppm Ba, 1000 ppm Sr. A 400 nA beam current was used to obtain trace element compositions at the rims of anorthite crystals and those edge regions were assumed to be near chemical equilibrium with the surrounding glass compositions. Further analytical and experimental details are given in Section 2.2.4.

Despite the above results, comparison of the overall SIMS D_{Ba} data with our adopted EMP rim analyses (Table A1.1) indicates acceptable agreement (everything within 30 %). Only composition 5 has a higher SIMS D_{Ba} than that from the rim EMP analyses by more than two standard deviations of the propagated standard deviations.

Five out of six compositions showed higher D_{Ba} using the SIMS data for crystal centers, which is consistent with some disequilibrium partitioning for the center data. However, unlike the EMP center-rim comparison above, there are likely systematic error differences between the SIMS and EMP data, so systematic offsets cannot be interpreted statistically. The effect of such systematic SIMS-EMP differences is illustrated by the D_{Sr} data in Table A1.1. With D_{Sr} approximately 1, all data are expected to be insensitive to disequilibrium partitioning effects. The D_{Sr} from SIMS are systematically higher than the rim EMP D_{Sr} by amounts ranging from 6 to 18 %. However, when regarding the measured standard deviations as uncertainties, the SIMS-EMP rim difference only exceeds 2 σ for composition 5 (as for Ba).

A1.2.3 Be Partitioning

Plagioclase/melt partition coefficients for Be have been determined by Bindeman et al. (1998), who measured natural Be abundances of approximately 50–500 ppb by ion microprobe in 1 atm experimental charges from Drake and Weill (1975). Those partition coefficients (D^{molar}) range from 0.17 ± 0.07 for an intermediate plagioclase composition ($An_{44.8}$) at the lowest experimental temperature of 1153 °C to 0.56 ± 0.08 in the most anorthitic ($An_{77.2}$) composition and highest temperature (1297 °C) of the study. The least square approximation parameters for Be partitioning according to their equation,

$$\mathrm{RT}\ln(\boldsymbol{D_i}) = \boldsymbol{a}\cdot\boldsymbol{X_{An}} + \boldsymbol{b}$$

are a = 28.2 ± 6.1 and b = -29.5 ± 4.1, in units of kJ. This predicts a Be partition coefficient of 0.90 for pure anorthite, well above the values measured in our study. Combined a and b parameter error yields a prediction uncertainty of ±0.2, but this fails to

reconcile the model with our measured partition coefficients at higher concentration levels. Caution is warranted because the systematic errors introduced in our data by the use of the quartz diorite glass TI-G as the SIMS standard are unknown.

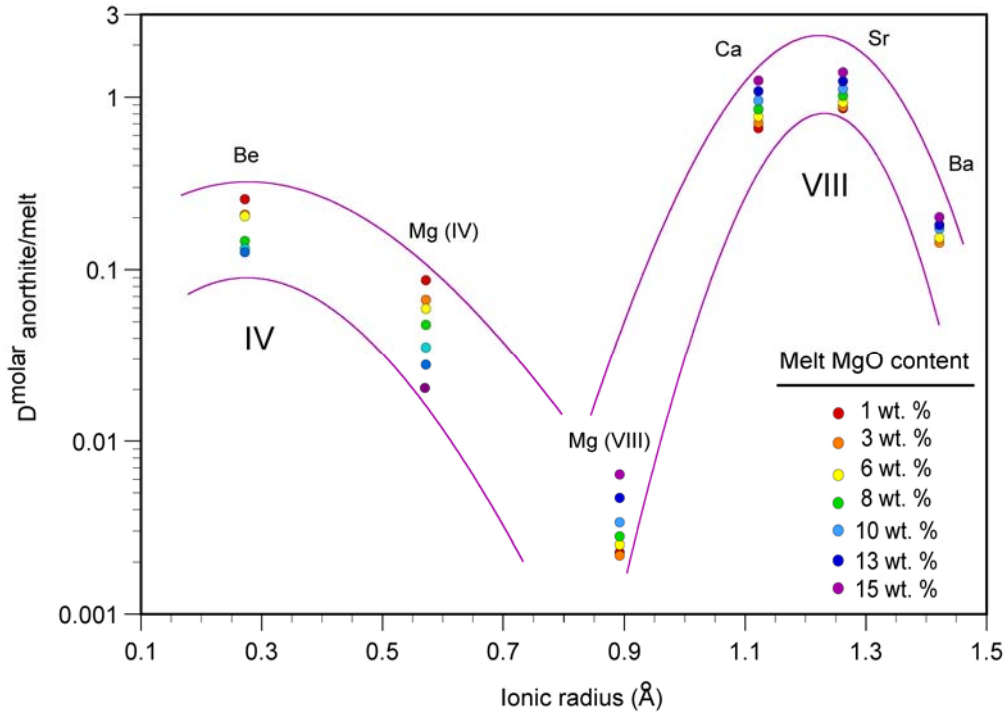

Figure A1.3. Anorthite/silicate melt divalent element partitioning of tetrahedral and cubic coordination site occupancy for CMAS2 compositions.

The Be partition coefficients measured in the compositions of this study show a systematic decrease from 0.27 in the least magnesian melt composition 2-1 (~1 wt. % MgO) to 0.13 in the 2-6 experimental charge, which contains an initial melt content of ~ 12 wt. % MgO. This trend mirrors that of the magnesium population calculated to partition onto the tetrahedral (IV-fold) site of the anorthite structure using equation (2.16) in Section 2.3.3, as may be expected since Be is tetrahedrally coordinated in plagioclases (Smith and Brown, 1988). Error bars are omitted for clarity in Figure A1.3, but 1 σ uncertainties for these partition coefficients are reported for bulk Mg in Table 2.3 of

chapter 2 and the last column of Table A1.1 for Be. The split of Mg into both tetrahedrally and octahedrally coordinated sites within the anorthite crystal lattice due to its intermediate size likely exists for a number of similar divalent cations with ionic radii between 0.55 and 0.66 Å, including Ni, Cu, Co, Cd, Zn, Fe, and Mn (Shannon, 1976).

A1.3 Major Element Crystal Homogeneity

Identifying the effect of melt composition on partitioning requires varying melt compositions of experimental charges while simultaneously holding temperature, pressure, and crystal chemistry constant. To verify that the major element compositions of the anorthites were not varying between experiments or within individual laths, points across transects of two crystals from each of the seven controlled cooling experiments in the CMAS2b suite were analyzed for CaO, Al_2O_3, and SiO_2 by electron microprobe using a synthetic anorthite standard, 25 nA beam, 15 keV, and 30 s on peak and 15 s background. The wt. % data plotted in Figure A1.4 indicate no major element crystal heterogeneity within analytical precision. Points furthest from the crystal centers that are elevated (Al_2O_3 and SiO_2) or low (CaO) are at the edges of the crystals and either represent partial or full analyses of the surrounding glass composition.

Figure A1.4 (next page). Major element traverses from rim to rim across representative anorthite crystals from CMAS2b experiments: (a) and (b) 2b-1-2, (c) and (d) 2b-2-2, (e) and (f) 2b-3-2, (g) and (h) 2b-4-2, (i) and (j) 2b-5-2, (k) and (l) 2b-6-2, and (m) and (n) from 2b-7-2. Error bars represent 1 σ analytical uncertainty; those not visible lie within symbol size shown.

Figure A1.4 (cont.)